Mixing performance of viscoelastic fluids in a kenics km in-line static mixer

Ramsay, J.; Simmons, Mark; Ingram, A.; Stitt, E.h.

DOI:
10.1016/j.cherd.2016.07.020

Document Version
Publisher's PDF, also known as Version of record

Citation for published version (Harvard):
Ramsay, J, Simmons, M, Ingram, A & Stitt, EH 2016, 'Mixing performance of viscoelastic fluids in a kenics km in-line static mixer', *Chemical Engineering Research and Design*, vol. 115, no. Part B, pp. 310–324. https://doi.org/10.1016/j.cherd.2016.07.020

Contents lists available at ScienceDirect

Chemical Engineering Research and Design

journal homepage: www.elsevier.com/locate/cherd

Mixing performance of viscoelastic fluids in a Kenics KM in-line static mixer

J. Ramsay[a], M.J.H. Simmons[a,*], A. Ingram[a], E.H. Stitt[b]

[a] School of Chemical Engineering, University of Birmingham, B15 2TT, UK
[b] Johnson Matthey Technology Centre, Billingham, TS23 1LB, UK

ARTICLE INFO

Article history:
Received 30 March 2016
Received in revised form 18 July 2016
Accepted 24 July 2016
Available online 29 July 2016

Keywords:
Mixing performance
Kenics
Static mixer
PLIF
Viscoelasticity
Fluid blending

ABSTRACT

The mixing of ideal viscoelastic (Boger) fluids within a Kenics KM static mixer has been assessed by the analysis of images obtained by Planar Laser Induced Fluorescence (PLIF). The effect of fluid elasticity and fluid superficial velocity has been investigated, with mixing performance quantified using the traditional measure of coefficient of variance CoV alongside the areal method developed by Alberini et al. (2013). As previously reported for non-Newtonian shear thinning fluids, trends in the coefficient of variance follow no set pattern, whilst areal analysis has shown that the >90% mixed fraction (i.e. portion of the flow that is within ±10% of the perfectly mixed concentration) decreases as fluid elasticity increases. Further, the >90% mixed fraction does not collapse onto a single curve with traditional dimensionless parameters such as Reynolds number *Re* and Weissenberg number Wi, and thus a generalised Reynolds number $Re_g = Re/(1 + 2Wi)$ has been implemented with data showing a good correlation to this parameter.

1. Introduction

The formulation of complex fluid products in industrial processes offers many challenges. Many common multiphase products, such as paints, inks or ceramic pastes, possess high levels of particulate solids loading, typically 45–55% by volume. Under shear conditions particle jamming can often occur, leading to highly viscous or viscoelastic rheologies. Due to the highly viscous consistency of these fluids, industrial blending operations take place under laminar flow conditions presenting significant challenges in achieving product homogeneity.

The primary complexity in material processing stems from the highly non-linear rheological behaviour these complex multiphase systems possess, manifesting as viscoelastic flow effects which, in addition to the high solid phase volume, can be attributed to polymer content in the liquid matrix and other multiphase components such as droplets and bubbles (Barnes, 2003). The interaction between viscoelasticity and continuous flow processes has received comparatively little attention in the open literature as most studies have focussed on batch stirred tank systems. Traditionally, these stirred tanks have been agitated using specialised impeller designs such as the anchor, helical ribbon (Ihejirika et al., 2007; Chavan, 1983; Chhabra et al., 2007; Jahangiri, 2007) or butterfly impeller (Ramsay et al., 2016) in order to perform the required mixing duty with viscoelastic fluids. However, batch systems possess many limitations, such as high energy demands and high labour costs due to operator intervention and process cleaning. It is therefore imperative to shift to continuous methods of processing, owing to their comparative reduced energy input and labour, smaller plant footprint enabling a greater degree of process intensification, and the ability for tighter process control allowing for a more consistent product output (Paul et al., 2003).

In recent years there has been significant interest in the performance of in-line static mixers, also known as motionless mixers, in both laminar and turbulent flow applications.

* *Corresponding author at*: School of Chemical Engineering, University of Birmingham, B15 2TT, UK.
E-mail address: m.j.simmons@bham.ac.uk (M.J.H. Simmons).
http://dx.doi.org/10.1016/j.cherd.2016.07.020

Nomenclature

Roman letters

a	power law pre-exponential factor s^{b+1}
b	power law exponent
C	concentration ($g\,L^{-1}$)
D	diameter (m)
El	elasticity number
f_D	Darcy friction factor
f_X	areal mixing fraction
G	greyscale
K_G	mixer shear rate constant
K_i	mixer mixing efficiency constant
K_L	mixer pressure drop ratio factor
n	number
L	length (m)
N_1	first normal stress difference (Pa)
P	pressure (Pa)
Q	flow rate ($m^3\,s^{-1}$)
Re	Reynolds number
Re_g	generalised Reynolds number
t	time (s)
u	superficial velocity ($m\,s^{-1}$)
Wi	Weissenberg number
X	areal mixing intensity

Greek letters

$\dot{\gamma}$	shear rate (s^{-1})
Δ	difference
ε	specific energy input ($J\,kg^{-1}$)
η	fluid apparent viscosity (Pa s)
λ	fluid relaxation time (s)
μ	fluid Newtonian viscosity (Pa s)
ρ	fluid density ($kg\,m^{-3}$)
σ	variance
τ	shear stress (Pa)
ψ	normal stress coefficient ($Pa\,s^{-2}$)

Static mixers consist of metallic inserts that fit into a pipeline and redirect flow in order to improve inter-material contact, which is beneficial in mixing systems ranging from simple blending operations through to chemical reaction and heat transfer (Paul et al., 2003). Implementation of these mixers into process lines is relatively straightforward: only standard pumping equipment is required for use as the mixer inserts into a pipeline although there will be an inevitable increase in pressure drop. Although many manufacturers offer a range of designs tailored to each application, the most common type under investigation in academic circles is the Kenics KM mixer (Chemineer, USA) which is comprised of a series of helically twisted elements. The simplicity of this mixer design has made it a favoured geometry for investigation, as its split-and-recombine design performs the standard Baker's transformation for mixing duties in laminar flow (Paul et al., 2003). Furthermore, the geometry is easily modelled in computational fluid dynamics (CFD) simulations, and has been the subject of several investigations with the aim of assessing flow structures within the mixer itself (Rahmani et al., 2006; van Wageningen et al., 2004; Rauline et al., 2000; Avalosse and Crochet, 1997; Regner et al., 2006; Saatdjian et al., 2012; Hobbs and Muzzio, 1998).

Some of the earliest investigations into static mixer performance by Shah and Kale (1991) and Chandra and Kale (1992) focussed exclusively on the pressure drop across the mixer with various fluids. Remarkably, despite limited literature on static mixer performance available at the time, viscoelasticity was also investigated. They found a significant increase in pressure drop as fluid elasticity increased at low Reynolds numbers with data fitting a polynomial type expression. Further, additional works (Li et al., 1997; Kumar and Upadhyay, 2008) have also attempted to fit pressure drop data to a variety of models, with some (Laporte et al., 2014) applying a stirred tank analogy using a power factor K_p in laminar flow. The design factor K_L, also known as the z-factor, is the most commonly used measure for mixer pressure drop ratio, and is defined as:

$$K_L = \frac{f_{D,mixer}}{f_{D,empty\,pipe}} = \frac{\Delta P_{mixer}}{\Delta P_{empty\,pipe}} \quad (1)$$

where f_D is the Darcy friction factor and ΔP the pressure drop. For the Kenics KM mixer, K_L is commonly taken as 6.9, a value determined for Newtonian fluids in laminar flow (Paul et al., 2003; Thakur et al., 2003). Other work has suggested that for non-Newtonian fluids the value of K_L is significantly lower than this (Alberini et al., 2013), and furthermore the presence of viscoelasticity may well produce significant deviation from this design parameter due to the existence of secondary flows perpendicular to the main flow direction; previous design parameters have been calculated based on the laminar flow of Newtonian fluids only.

Assessing the impact of viscoelasticity on processes possesses many challenges. Owing to their non-linear behaviour, it is often difficult to define a single parameter to fully characterise flow behaviour. Most studies apply traditional approaches, with correlations of Reynolds number, Re, and viscoelastic Weissenberg number, Wi, however these in isolation cannot fully describe the flow conditions as they ignore the relative effects of elasticity and inertia respectively. Some studies have implemented a combined approach, using dimensionless groups such as the Elasticity number El (Stokes, 1998; Ozcan-Taskin and Nienow, 1995), or more recently the generalised Reynolds number Re_g, which seeks to correct the viscous stress term present within the Reynolds number for elastic effects (Bertrand et al., 2002). All of these recent studies applied optical flow measurement techniques such as Particle Image Velocimetry (PIV) (Faes and Glasmacher, 2008; Hall et al., 2005; Szalai et al., 2004; Zalc et al., 2001; Pianko-Oprych et al., 2009; Gabriele et al., 2009; Stobiac et al., 2014), Planar Laser-Induced Fluorescence (PLIF) (Kling and Mewes, 2004; Arratia and Muzzio, 2004; Alvarez et al., 2002; Chung et al., 2009; Guillard et al., 2000) or dye decolourisation techniques (Shervin et al., 1991; Fradette et al., 2007) and were focussed on viscoelastic mixing behaviour in stirred tanks; to date there have been very few publications investigating viscoelastic fluids within static mixers (Chandra and Kale, 1992; Li et al., 1997). These optical methods all require transparent fluids which can be a limitation, however another non-invasive technique, Positron Emission Particle Tracking (PEPT) which is suitable for opaque fluids, has also been applied to static mixers for Newtonian and non-Newtonian inelastic fluids (Rafiee et al., 2011). The technique reveals velocity fields and shear rates in addition to mixing measures such as segregation index (Mihailova et al., 2015). For local mixing performance, PLIF has become the experimental method of choice for a range of mixing

applications. The mixing region is illuminated with a laser sheet perpendicular to the camera: the fluorescent intensity of a dye (injected into one of the mixing phases) is used to infer a map of the instantaneous and transient concentration field.

Most of these techniques have assessed mixing performance using the traditional method of intensity of segregation, as determined by the coefficient of variance CoV within the flow. However, recent studies (Kukukova et al., 2009) have shown CoV to be insufficient in describing the complete mixing condition of a fluid as it does not include the scale of segregation, the other of the two primary measures of mixing stated by Danckwerts (1958). In order to address this deficiency, Alberini et al. (2013) developed the areal distribution method which combines scale and intensity of segregation in a frequency distribution of mixedness. Originally developed for static mixer geometries, the technique has also been applied to stirred tanks (Stamatopoulos et al., 2015).

Although there has been much investigation into characterising viscoelastic fluids, understanding the application of these fluids in processes remains difficult. For example, the literature is divided as to whether secondary flows, generated due to normal stress differences present only in viscoelastic flow, enhance or inhibit mixing performance: several works argue that the additional transport in the non-primary flow direction aids convective mixing processes and thus improves performance (Stobiac et al., 2014; Fradette et al., 2007; Fontaine et al., 2013), whilst others claim that the same transport reduces this performance due to the solid-like portions of the flow being less readily mixed (Ramsay et al., 2016; Ozcantaskin and Nienow, 1995; Seyssiecq et al., 2003). As the viscoelasticity of multiphase fluids remains poorly characterised and its effect on processes is still unknown due to the complexity of decoupling viscous and elastic effects, it is desirable to investigate a more idealised viscoelastic fluid to understand the underlying flow phenomena. More specifically, it is necessary to isolate the well-documented effect of varying viscosity from the little understood effect of varying elasticity, which is achieved by using a class of viscoelastic fluid known as the "Boger" fluid, typically made from the addition of a dilute polymer to a Newtonian solvent (Boger and Yeow, 1992; Mackay and Boger, 1987). These fluids possess a constant viscosity and an elasticity that can be controlled through varying polymer concentration. They also have the benefit of being optically transparent and have been used in several flow visualisation investigations (James et al., 2012; Magda et al., 1991; Stokes et al., 2001; Stokes and Boger, 2000). As the fluid viscosity and elasticity of Boger fluids can be controlled independently they are suitable candidates for mimicking a range of other more complex materials (Ramsay et al., 2016).

This work seeks to characterise the interaction between viscoelastic materials and continuous in-line static mixers through assessment of blending performance and energy efficiency. Qualitative and quantitative mixing performance has been obtained using PLIF measurements, whilst pressure drop measurements enable calculation of energy input. Mixer behaviour has been examined using fluids of increasing rheological complexity through use of transparent Newtonian and Boger fluids with the same base fluid viscosity. Key performance parameters such final mixing quality assessed through areal analysis and coefficients of variance (CoV) have been calculated over a range of industrially relevant process conditions and compared to a range of dimensionless hydrodynamic parameters and process energy inputs in order to determine the underlying controlling mechanisms for mixing performance.

2. Methods and materials

2.1. Experimental set-up

Experiments were performed in a continuous flow rig as displayed in Fig. 1. The main flow into a 12.5 mm ID pipe was delivered from a 20 L header tank via a gear pump (Liquiflow) powered by a motor drive (Excal Meliamex Ltd.). A secondary flow stream dyed with 0.5 mg L^{-1} Rhodamine-6G (Sigma Aldrich, UK), which acts a passive scalar for local concentration measurement, was delivered from a pressurised 5 L vessel via a gear pump (GB-P35, Cole-Parmer, UK). Flow rates were measured from an in-line flowmeter (Krone) in the main flow and indirectly from pump speed via previous calibration measurements for the secondary stream. The secondary stream was injected via a coaxial nozzle, 4 mm I.D., at a flow ratio of 10% of the total stream flow rate in order to achieve isokinetic conditions between the main and secondary streams. The combined stream then passed through a six element ½" (internal diameter 14.7 mm) diameter Kenics KM static mixer (Kenics, USA), with all six elements at 90° to the preceding element. Downstream of the mixer outlet was a transparent pipe section, consisting of a ½" I.D. unplasticised poly(vinyl chloride) (uPVC) pipe encased in a transparent poly(methyl methacrylate) square-section box filled with water. At the exit of the transparent section a tee-piece was fitted, with the branching outlet dumping to the fluid drain whilst the other outlet was capped with a poly(methyl methacrylate) viewing window permitting observation of the upstream pipe cross-section when illuminated with laser light. Pressure drop measurements were taken ex situ through fitting 1 bar Keller S35X pressure transducers (Keller, UK) at the mixer inlet and outlet. The flow rates Q of 68.4 to 136.8 L hr^{-1} implemented in this study are typical of industrial processing superficial velocities for the pipe diameters studied. Reynolds number fall well below the critical value of $Re = 2100$, with values of $Re < 30$ existing in all cases. Table 1 displays the experimental conditions.

2.2. Fluid rheology

A class of transparent viscoelastic fluids known as Boger fluids were used in this study in order to provide viscosities and elasticities in a similar range to industrially relevant viscoelastic materials. Fluids were formulated using a bench-top laboratory mixer (Heidolph RZR-2102, Heidolph UK). Dilute polymer solutions of poly(acrylamide) (Sigma Aldrich, UK) in aqueous glycerol (ReAgent, UK) were formulated in 20 L batches, with water used to make up the remainder. Sodium chloride salt (Sigma Aldrich, UK) was added to aid polymer dissolution during fluid formulation. Rheological characterisation was performed using a Discovery Hybrid HR-2 rheometer (TA Instruments, USA) using a 40 mm 4° cone and plate geometry over a range of shear rates, $\dot{\gamma}$, between 0.1 and 1000 s^{-1}. This shear rate range was selected to capture the maximum theoretical shear rate (found at the pipe wall) for the static mixer at experimental conditions using the design correlation:

$$\dot{\gamma}_W = \frac{K_G u}{D} \quad (2)$$

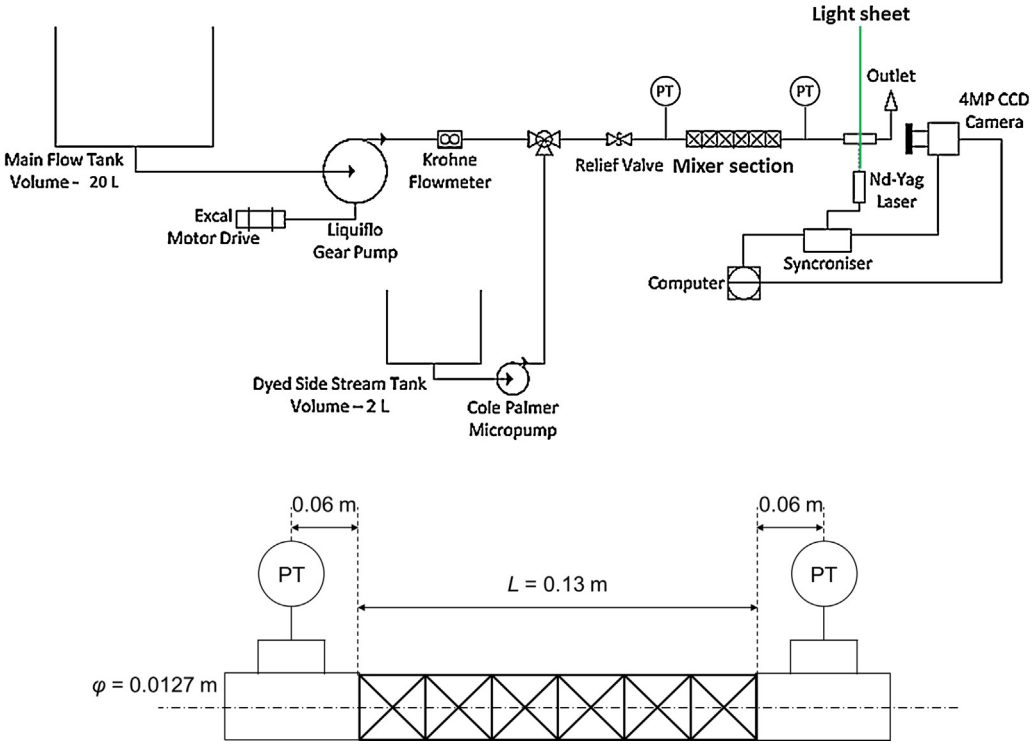

Fig. 1 – (a) Equipment set-up diagram; (b) static mixer section dimensions.

Table 1 – Experimental conditions for PLIF experiments.

Main stream flow rate, Q ($L\,h^{-1}$)	Secondary stream flow rate, Q_S ($L\,h^{-1}$)	Total flow rate, $Q_T = Q + Q_S$ ($L\,h^{-1}$)	Superficial velocity, u ($m\,s^{-1}$)	Newtonian mixer wall shear rate $\dot{\gamma}_W$ (s^{-1})	Newtonian Reynolds number, *Re*
61.6	6.8	68.4	0.15	331	14.5
82.1	9.1	91.2	0.20	441	19.4
123.1	13.7	136.8	0.30	661	29.0

where K_G is the mixer shear rate coefficient (28 for a Kenics KM) (Paul et al., 2003), u the superficial flow velocity ($m\,s^{-1}$) and D the mixer diameter (m).

Normal stress differences, the differences in the principal normal stress components of the stress tensor (Barnes, 2000), were directly measured during the acquisition of shear stress versus shear rate data on the same instrument through axial force measurement. The fluid relaxation time, λ, the primary measure of material viscoelasticity, was calculated as a function of shear rate from the ratio of first normal stress difference N_1 to viscosity and fitted to a power law model (Ozcantaskin and Nienow, 1995):

$$\lambda(\dot{\gamma}) = \frac{\psi_1(\dot{\gamma})}{2\eta(\dot{\gamma})} = \frac{1}{2\eta(\dot{\gamma})}\left(\frac{N_1(\dot{\gamma})}{\dot{\gamma}^2}\right) \quad (3)$$

$$\lambda = a\dot{\gamma}^b \quad (4)$$

where ψ_1 is the first normal stress coefficient, η the fluid apparent viscosity, N_1 the first normal stress difference, $\dot{\gamma}$ the shear rate, while a and b are constants. The compositions of the model fluids used and their rheological parameters can be found in Table 2. Fig. 2 displays the rheological data obtained.

As Fig. 2a shows both Boger fluids possess approximately constant viscosity across the measured range. Additionally, these values are similar, indicating that glycerol concentration controls the baseline material viscosity and thus allows us to assess elasticity independently. The elastic responses

Table 2 – Fluid compositions and rheological parameters.

	Glycerol	Boger A	Boger B
Polyacrylamide (wt.%)	–	0.01	0.02
Glycerol (wt.%)	90.00	90.00	90.00
Water (wt.%)	10.00	8.33	8.32
Sodium chloride (wt.%)	–	1.66	1.66

Fluid	Viscosity, η (Pa s)	Relaxation time pre-exponential factor, a (s^{b+1})	Relaxation time power law exponent, b
Glycerol	0.188 (±0.014)	–	–
Boger A	0.195 (±0.019)	87.76 (±18.49)	−1.81 (±0.02)
Boger B	0.164 (±0.024)	157.36 (±31.12)	−1.78 (±0.04)

are shown in Fig. 2b; for both materials N_1 increases with increasing shear rate, however the rate of increase reduces at increasing shear rates indicating that instead of the expected quadratic N_1 response that a "true" Boger fluid should possess, which is only valid at low shear rates, a power-law type model is more suitable. However, it can be seen that at all measured values the response of Boger A displays lower values of N_1, thus indicating that Boger A possess a lower elasticity than Boger B; this is further observed in the fluid relaxation times which also fit a power law model.

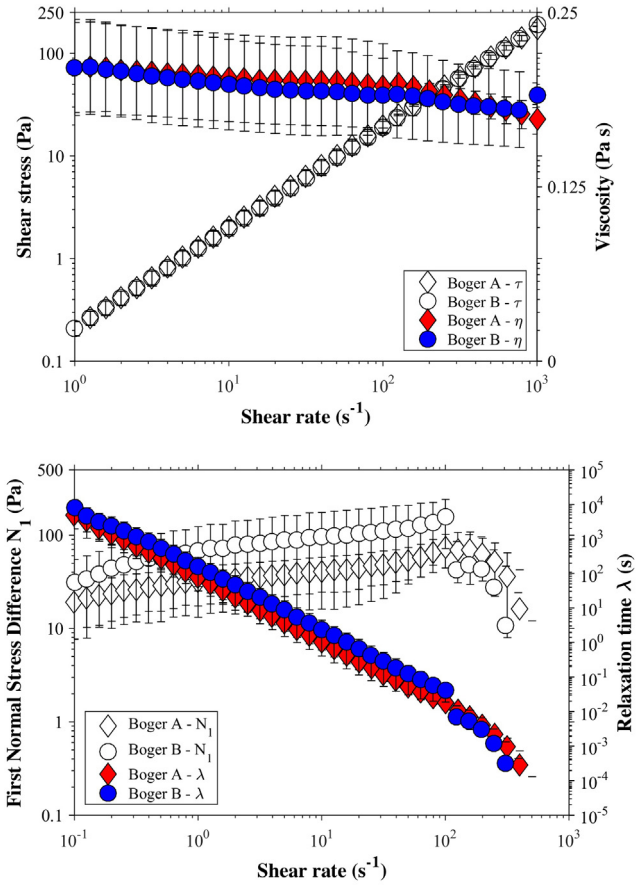

Fig. 2 – (a) Shear stress τ and viscosity η versus shear rate $\dot{\gamma}$ for Boger fluids; (b) first normal stress differences N_1 and relaxation times λ for Boger fluids.

At the experimental conditions used for both PLIF and pressure drop experiments, experimental Reynolds numbers *Re* vary between 10 and 30 and are defined as:

$$Re = \frac{\rho u D}{\eta} \tag{5}$$

where ρ is the fluid density, with actual values of superficial velocity and measured internal diameter used in this calculation.

Additionally, the fluid elasticity has been calculated through calculation of the dimensionless Weissenberg number *Wi*, which is defined as the ratio between the material and process characteristic timescales at steady state. The value has been calculated by:

$$\mathrm{Wi} = \lambda \dot{\gamma}_W \tag{6}$$

where λ is the material relaxation time. This can also be coupled to the Reynolds number in order to provide an overall dimensionless parameter to describe the flow. A commonly implemented definition is that of the Elasticity number *El*, which is defined as the ratio between elastic and inertial forces within the flow:

$$El = \frac{\mathrm{Wi}}{Re} \tag{7}$$

Further, Bertrand et al. (2002) have proposed a new method for a combined approach, through implementing a generalised Reynolds number Re_g. This aims to account for fluid elasticity through correcting the viscous term in the Reynolds number definition, such that:

$$Re_g = Re(1 + 2\mathrm{Wi})^{-1} \tag{8}$$

For an elastic fluid, the value of Re_g is always lower than the standard definition of *Re* for $Wi > 0$. In the Newtonian case ($Wi = 0$), $Re_g = Re$. This approach can only be applied to second-order fluids such as Boger fluids, as this definition of Re_g relies on a second-order stress response. The derivation of Re_g is shown in Appendix A.

2.3. Power input

Process power input was determined from pressure drop measurements over a range of fluid velocities. Specific energy input at a given flow condition is given by:

$$\varepsilon = \frac{\Delta P}{\rho} \tag{9}$$

where ε is the specific energy input (J kg^{-1}) and ΔP the pressure drop (Pa).

In laminar flow, the theoretical empty pipe pressure drop is calculated from the Hagen–Poiseuille equation:

$$\Delta P_{empty\ pipe,\ theoretical} = \frac{128\eta L Q}{\pi D^4} = \frac{32\eta L u}{D^2} \tag{10}$$

where *L* is the length of the measurement section (m). Further, the empty pipe Darcy friction factor f_D can be calculated by:

$$f_D = \frac{64}{Re} = \frac{\Delta P}{\left(\frac{L}{D}\right)\left(\frac{1}{2}\rho u^2\right)} \tag{11}$$

Mixer friction factor and pressure drop ratio K_L have been calculated according to Eq. (1). Both the standard Reynolds number definition and the generalised Reynolds number shown in Eq. (8) have been implemented in order to assess deviation from the predicted pressure drop values.

2.4. Planar laser induced fluorescence (PLIF)

PLIF was performed at all experimental conditions (Table 1). A 532 nm Nd-YAG laser (nanoPIV, Litron, UK) operating at 2.07 Hz was fitted with −100 mm cylindrical lens and a 500 mm focussing lens in order to project a planar sheet, of thickness less than 0.1 mm, through the transparent mixer outlet section. A 12-bit 4MP CCD camera (TSI, USA) captured images synchronous to the laser pulses, with timings controlled via a synchroniser (TSI 610035) linked to a personal computer operating Insight 4G software for image acquisition (TSI, USA). The image resolution was 22 μm pixel^{-1}, hence all measurements of mixing performance assess the macromixing quality only. 20 images were recorded at all conditions equating to 9.67 s of imaging, which is of the order of several fluid relaxation times at all conditions.

Rhodamine-6G was added to the secondary flow stream as the fluorescent tracer. A 545 nm cut-off lens was fitted to the camera to act a high-pass filter, eliminating all light but that fluoresced by the dye ($\lambda = 560$ nm). In order to select a suitable concentration of fluorescent dye, calibration experiments were performed by filling the pipe section with dye of a set concentration. An example calibration curve is displayed in Fig. 3; it was observed that the local greyscale

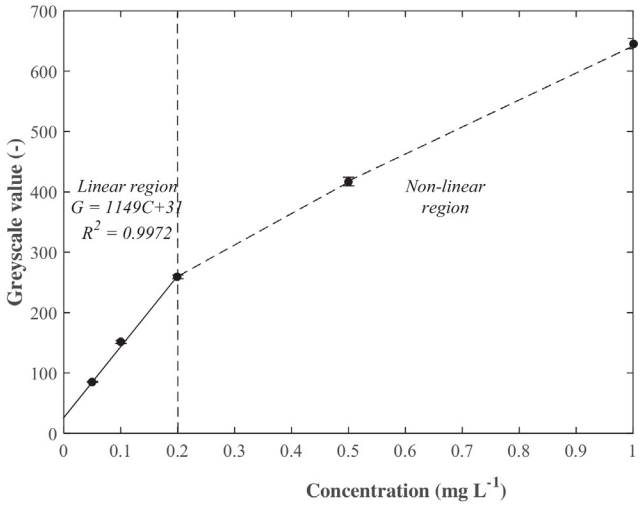

Fig. 3 – Example PLIF calibration curve of rhodamine-6G concentration against average image greyscale value.

values did not vary significantly across the image and therefore a single average greyscale has been used to construct the greyscale-concentration relationship. As the relationship between greyscale value and dye concentration is linear below a critical dye concentration, it is possible to calculate local concentrations and thus mixing performance.

From PLIF data, areal concentration distributions are calculated using bespoke MATLAB code. The method is explained in full in Alberini et al. (2013); only an abridged version is presented here for brevity. The perfectly mixed concentration (or grayscale) value $\bar{C}$ is calculated from a theoretical mass balance across the mixer. Using the principle that material that is mixed to an arbitrary degree, X, will possess concentrations in the range of $[1-(1-X)]\bar{C}$ to $[1+(1-X)]\bar{C}$, it is possible to split the observed images into regions of known mixedness, e.g. 80–90% mixed, 50–60%, >90%, etc. The MATLAB DipImage toolbox (Delft University of Technology, The Netherlands) is implemented to isolate regions of the image within the same concentration range, and the number of pixels within each concentration is summed to give the fraction f_X of the image in the given mixedness quality range.

Additionally, in order to provide a comparison to the standard mixing measurements, the coefficient of variance CoV for the image is calculated.

$$CoV = \frac{\sigma}{\bar{C}} \tag{12}$$

where σ is the local concentration variance ($g L^{-1}$) and $\bar{C}$ is the perfectly mixed concentration ($g L^{-1}$). The variance is calculated by:

$$\sigma = \frac{1}{1-n}\sum_{i=0}^{n}\left(C'_{a,i}-1\right)^2 \tag{13}$$

where n is the maximum number of data points (in this case the total number of locations), and $C'_{a,i}$ is defined as:

$$C'_{a,i} = \frac{C_{a,i}-C_0}{\bar{C}-C_0} \tag{14}$$

where $C'_{a,i}$ is the normalised concentration of component a at location i, $C_{a,i}$ is the concentration at location i, and C_0 and $\bar{C}$ the initial and fully-mixed conditions respectively. With respect to the timescales involved, time $t = 0$ s was arbitrarily determined as the time that the first image was acquired at a given flow condition.

The coefficient of variance can be normalised to a reduced coefficient of variance CoV_r, which displays the reduction in CoV with respect to the inlet:

$$CoV_r = \frac{CoV}{CoV_0} \tag{15}$$

where CoV_0 is the initial coefficient of variance, calculated as 3.0 for a flow addition of 10% ({Paul, 2003 106/id}).

3. Results

3.1. Pressure drop data

The pressure drop measurements across the Kenics KM mixer for all fluids are shown in Fig. 4. Theoretical pressure drops have been calculated from Eqs. (10) and (1) assuming Newtonian behaviour and using the reported mixer K_L value of 6.9; confidence bounds of ±17% (Paul et al., 2003) have been implemented on friction factor f_D plots.

It can be observed that the pressure drops are higher than predicted by the combined Hagen–Poiseuille Eq. (10) and mixer K_L for laminar flow for all fluids, with glycerol, the Newtonian fluid, displaying a lower increase than both Boger A and Boger B. There appears to be a further increase at high values of Re indicating a tailing off effect. This can be attributed to the viscoelasticity these fluids exhibit which predicts an additional pressure drop due to the normal stress components of the stress tensor and elastic energy storage, which is consistent with the findings of Chandra and Kale (1992). Consequently, the apparent Darcy friction factors f_D calculated from the pressure drop data via Eq. (11) are significantly higher than those predicted by the Newtonian correlation with Reynolds number. This suggests that the Boger fluids may possess much lower Reynolds numbers than those calculated for the Newtonian definition; it is postulated that this may be due to the fluid elasticity affecting the flow pattern within the mixer and therefore changing the flow regime, as previously observed in swirling viscoelastic flows (Stokes, 1998). Therefore, it is necessary to investigate the variation of pressure drop and friction factor with the generalised Reynolds number, which corrects for elastic effects through incorporation of the Weissenberg number into the viscous term.

When the measured Darcy friction factors are plotted against the generalised Reynolds number Re_g as shown in Fig. 5, the data approaches a single curve, albeit with a significant deviation at low values of Re_g. This can be attributed to the over-prediction of the mixer wall shear rate, and thus that the vendor value of $K_G = 28$ may be unsuitable for non-Newtonian fluids. It has been observed in stirred vessels that viscoelasticity significantly alters the flow field and therefore features local shear rates differing from those seen in a Newtonian fluid of equivalent viscosity (Ramsay et al., 2016). Additionally, it has been reported that for various impeller designs a viscoelastic Metzner-Otto constant different in value to that used for inelastic fluids is required to fit viscoelastic data to Newtonian fluids (Bertrand et al., 2002); in static mixers the equivalent parameter is K_G. However, at present there is no experimental measurement of local flow fields with viscoelastic fluids in a Kenics KM mixer and as such the exact value of K_G is currently unknown and therefore the exact cause of this tailing

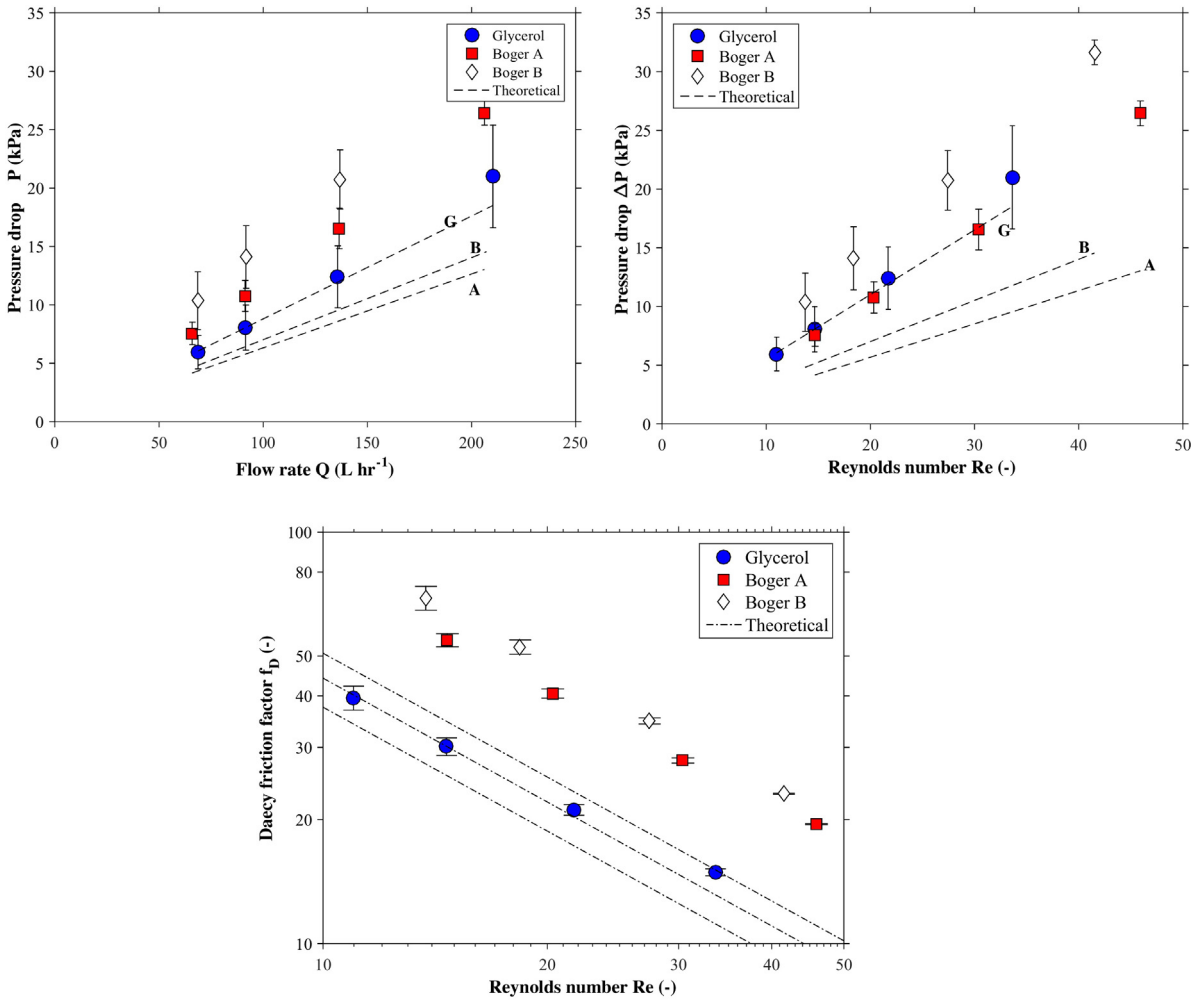

Fig. 4 – Pressure drop variation: (a) flow rate Q; (b) Reynolds number *Re*; (c) Darcy friction factor f_D.

effect remains unknown. It is speculated that the extensional viscosity may contribute to a change in the reported K_G value. Grace (1982) described droplet break-up in the same mixer, evaluating the extensional shear rate as a function of wall shear rate and concluded that, for Newtonian immiscible systems, the extensional viscosity is a governing parameter and is approximately equal to the pipe wall shear rate. Though valid for Newtonian and inelastic fluids, it has been shown that the extensional viscosity of viscoelastic fluids is significantly greater and varies across a range of shear rates (Stokes, 1998). Extensional viscosity data is unavailable for the Boger fluids investigated here and as such the impact of extensional shear on pressure drop and measured K_G value is unknown.

3.2. *Striation patterns*

It can be observed that there is a significant difference between the mixing patterns of the Newtonian glycerol and viscoelastic Boger fluids at a given superficial velocity. Primarily, the Newtonian fluid preserves the laminated striation pattern typical

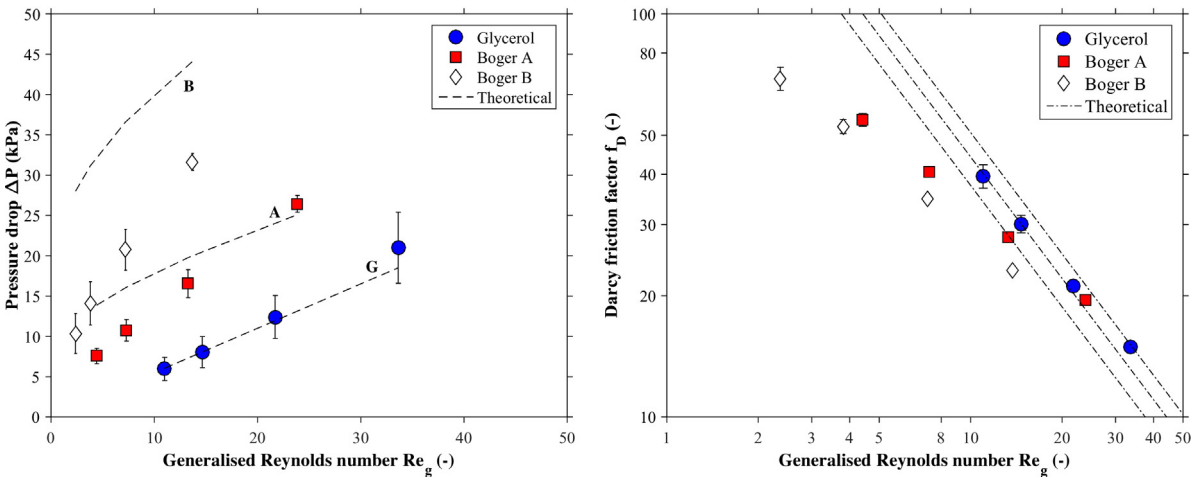

Fig. 5 – Pressure drop variation with generalised Reynolds number Re_g: (a) pressure drop ΔP; (b) Darcy friction factor f_D.

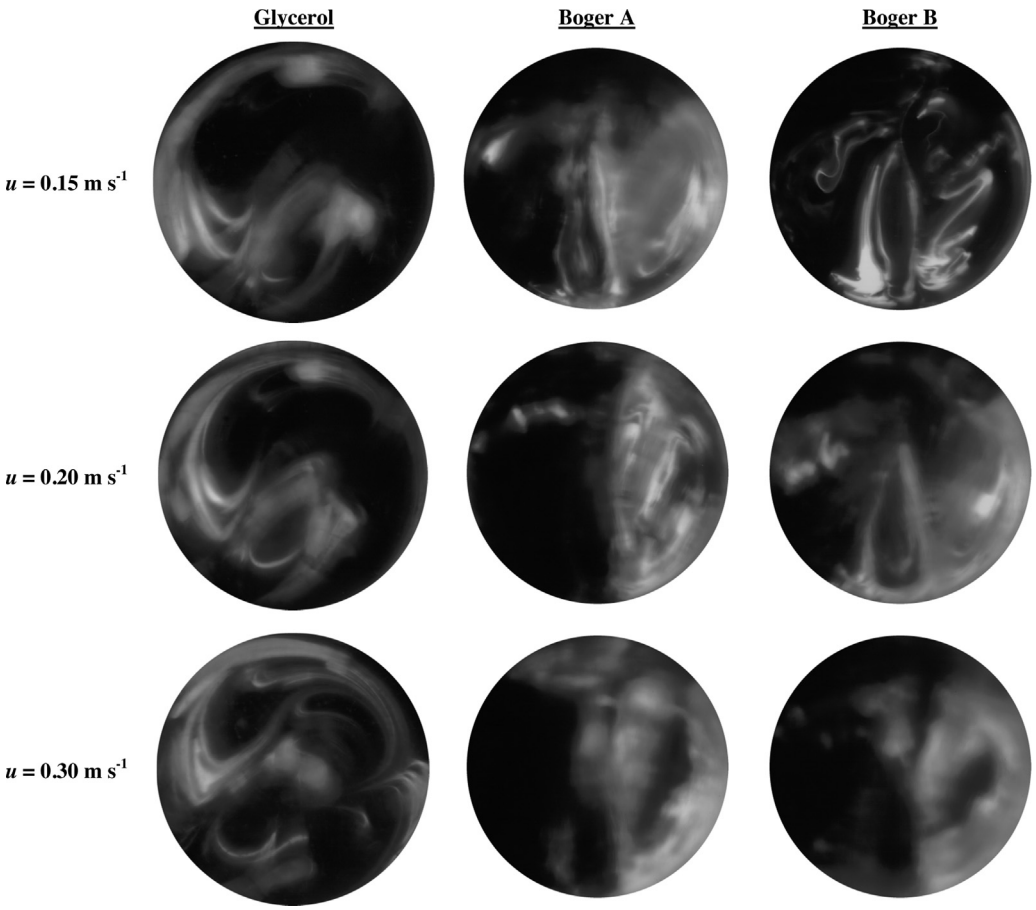

Fig. 6 – Striation patterns at mixer outlet, $t = 4.84$ s.

of a KM mixer at all velocities, whilst both Boger fluids deviate from this significantly at increasing velocities. Although evidence of this structured striation pattern exists at low velocities, as velocity increases both Boger fluids display a dual effect of both a slight "clouding" of the flow, as well as regions of greater greyscale intensity, and therefore local concentration, that do not conform to the expected Newtonian behaviour. The shape of the high intensity regions appears in two varieties: the first are spots which possess an elliptical shape close to a circular geometry, whilst the second appears in long elongated stretches as thinner single striations. The former is indicative of more solid-like behaviour in the flow persisting along the mixer length with a region of largely unmixed material not shearing into its surroundings. The latter structure is indicative of liquid-like behaviour, although the high dye concentration indicates a lack of material transfer from these striations. It is postulated that both of these deviations from Newtonian behaviour derive from the fluid elasticity, with the more elastic Boger B displaying a greater tendency towards these structures. Further, it can be noted for both viscoelastic fluids the tendency for the spot behaviour increases with increasing flow velocity, whilst the individual striation stretching occurs at lower velocities.

A further observation is that in the viscoelastic fluids there appears to be a tendency for the tracer to remain on one side of the mixer outlet, with the left hand side of the images in Fig. 6 showing poorer levels of mixing than the right. This is not observed in the glycerol data, with striation patterns visible across the entire section, albeit with large regions of undyed and therefore unmixed material. This could be caused by bypassing the initial mixing element, however as the experimental set-up was not changed between different fluid passes and glycerol does not show this effect this seems extremely unlikely. It perhaps suggests that, owing to the non-circular flow cross section of the Kenics KM mixer, secondary flow systems are present. This is typical of viscoelastic fluids which possess normal stress differences, most commonly the first normal stress difference N_1, as these act perpendicular to the main flow and as such set up secondary flow loops.

It should be stated at this point that based primarily on quantitative data, it is apparent that the overall mixing quality in all cases is poor. This is to be expected as the 6-element mixer is a relatively short design, and is operating at the low end of industrial velocities. As it should be expected that the number of striations at the outlet of a KM mixer should be simply 2^n, where n is the number of mixing elements, only 64 striations should be present in all cases. However, previous work has shown that velocity affects striation numbers and structure (Alberini et al., 2013, 2014). Further final mixing quality, usually a 90% mixed confidence interval, for this mixer is defined by the reduced coefficient of variance CoV_r (0.1 for the 90% mixedness case) and is linked to mixer performance through the parameter K_i (0.87 for a Kenics KM (Paul et al., 2003)), indicating a mixer length to diameter ratio L/D of:

$$CoV_r = \frac{CoV}{CoV_0} = K_i^{L/D}, \quad \frac{L}{D} = \frac{\log CoV_r}{\log K_i} = 16.5 \tag{16}$$

This would require 0.31 m of pipe, i.e. 14 mixer elements to achieve this mixing quality. However, it has previously been shown that using CoV in isolation is insufficient to fully

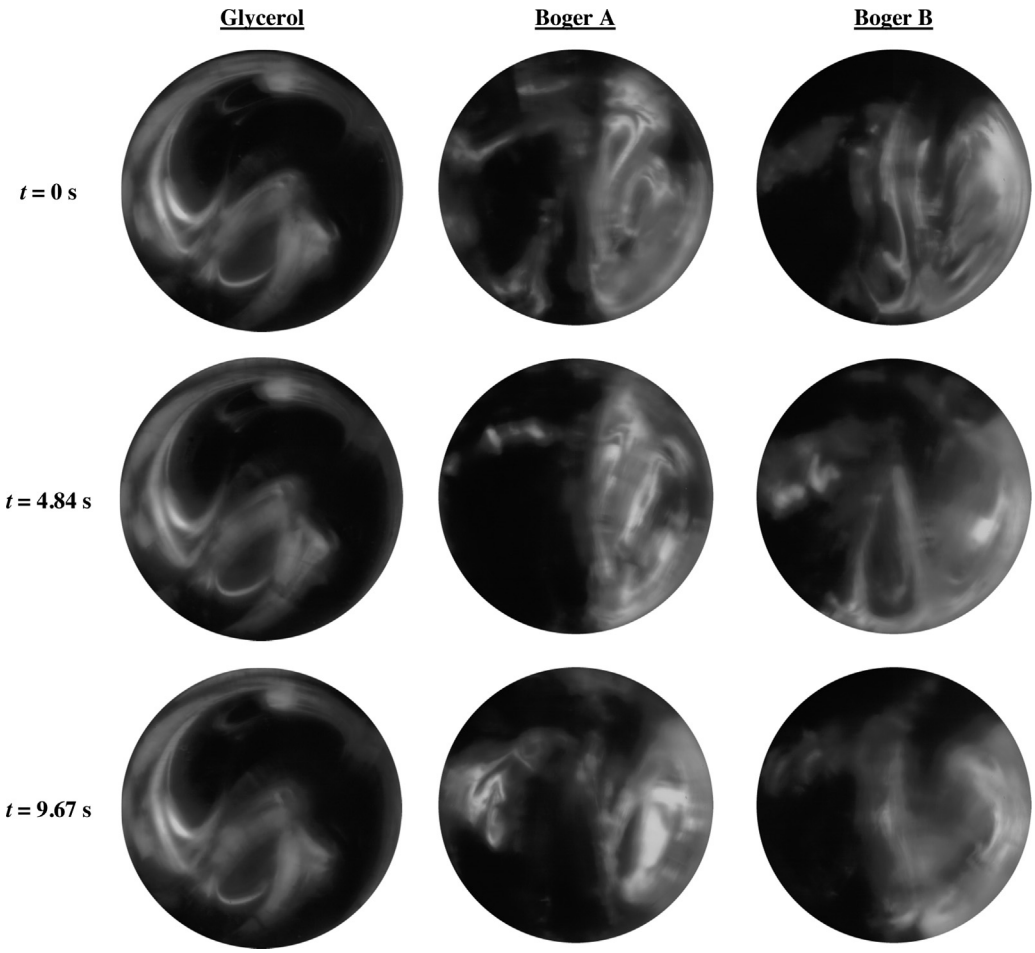

Fig. 7 – Variation in striation patterns at mixer outlet over time, $u = 0.2\,m\,s^{-1}$.

describe mixing performance (Alberini et al., 2013; Kukukova et al., 2008, 2009, 2011), so therefore the areal analysis of the raw data must be assessed.

3.2.1. *Time variation*

Previous studies in laminar flow with Newtonian and non-Newtonian inelastic fluids have shown the flow to be time invariant, with local greyscale values exhibiting negligible variation from frame to frame (Alberini et al., 2013, 2014). This invariance previously allowed for a single image at an arbitrary time to be analysed to determine mixing performance. However, for both the Boger fluids studied here this is not the case. Over the image acquisition period, the striation pattern at the mixer outlet varied significantly. Further, as the superficial flow velocity increased the pattern variation also became more pronounced. Fig. 7 displays the variation for Boger fluids A and B. Additionally, the statistics for both viscoelastic fluids are displayed in Fig. 8.

The time variation is most clearly seen in the *CoV* values. Significant variation over time can be observed, with *CoV* values varying by up to 20% of the mean of all values for a given experimental condition, with Boger B possessing the greatest statistical deviation from the mean. The same variation can be observed in the 90% mixed fraction data, with a maximum of 35% deviation from the mean also observed. The data also shows a periodicity around a central value, indicating that a pseudo-state had indeed been attained by the point of image acquisition. Table 3 displays the averages of the 90% mixed fractions and coefficients of variance for all conditions, with standard deviations displayed in brackets.

This temporal variation can only be attributed to the presence of elastic instability, due to local differences in relaxation time arising from the varied local shear rates within the mixer. Previous work discovered that for swirling flows in stirred vessels a characteristic flow map between Reynolds number *Re* and Weissenberg number *Wi* governed the shift from elastically driven flow to inertially driven (Stokes, 1998; Stokes et al., 2001). The values of these parameters in this study are comparable to those indicative of unsteady flow, indicating that the flow structures observed will not be constant over time. This can only be ascribed to the generation of normal stresses which act to destabilise the inertial flow.

Owing to this temporal variation, the mean and standard deviation of the mixing quality has been assessed; averages converge to a single value using a minimum of 15 images, thus the full set of 20 images has been used to obtain averages and standard deviations for each image statistic in order to compare the data further.

3.3. *Statistical analysis*

3.3.1. *Areal analysis and coefficients of variance*

The areal distributions shown in Fig. 9 display the time-averaged areal distributions, whilst Fig. 10 displays coefficients of variance for all fluids at constant velocity. Please note the scale; an upper limit of 25% has been implemented to improve clarity of the more important higher mixing fractions (>60%).

For a given velocity, the *CoV* always increases from Newtonian glycerol to viscoelastic Boger fluids. However, as velocity

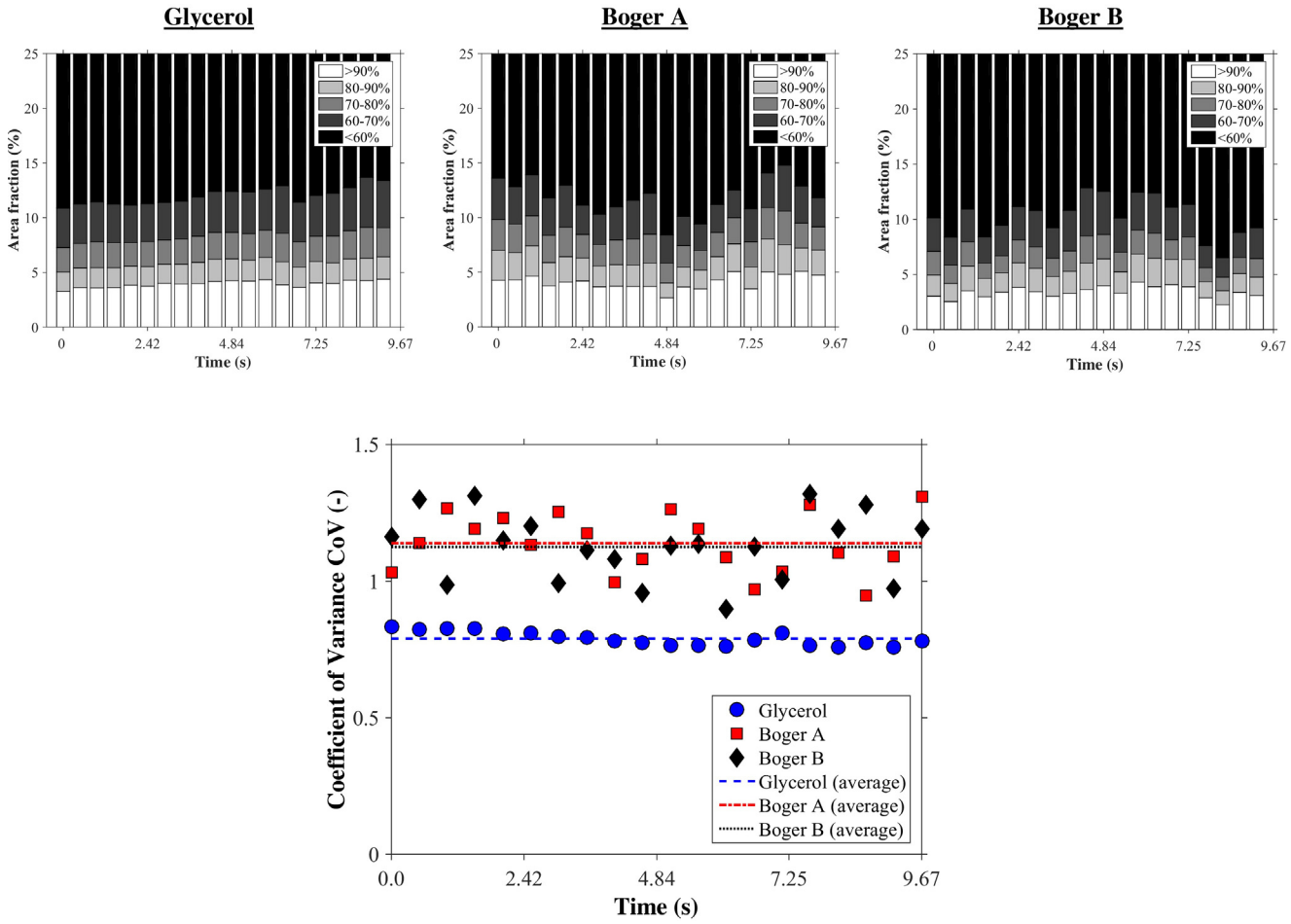

Fig. 8 – Time variation statistics: (a) area fraction; (b) coefficient of variance (CoV); dotted lines indicate mean values.

increases CoV decreases in glycerol whilst increasing in the Boger fluids. As previously stated, the use of CoV alone may not be representative of the mixing performance of complex flow structures and therefore the areal mixing fractions must be assessed to give a more complete picture of the performance. When the area fractions are studied, in particular the 90% mixed fraction, it can be observed that there is a monotonic trend in the size of this fraction as elasticity increases, with a slight decrease observed from glycerol to Boger A to Boger B at all conditions. This suggests that there is a weak effect of elasticity on mixing performance, with fluid elasticity inhibiting distributive mixing processes. When the values of the other mixed fractions (except < 60%) are observed, it can additionally be seen that as elasticity increases the area fractions each decrease. As with the 90–100% mixed fraction, this indicates that increasing elasticity inhibits mixing performance, with a greater tendency for more solid-like regions of flow to form that do not readily mix with the surroundings (Fig. 11).

When assessing the effect of velocity on each fluid individually, it can be seen that the trends in CoV do not follow the same pattern from fluid to fluid. Whilst glycerol displays a decrease in CoV as velocity increases, Boger A displays an increase followed by a large decrease whilst Boger B displays a continual increase as velocity increases. However, the same is not true of the area fractions for each fluid. It can be observed that whilst for glycerol the fraction of the 60% and greater mixedness levels all increase, both Boger fluids behave in a different manner. Boger A appears to show only a very slight

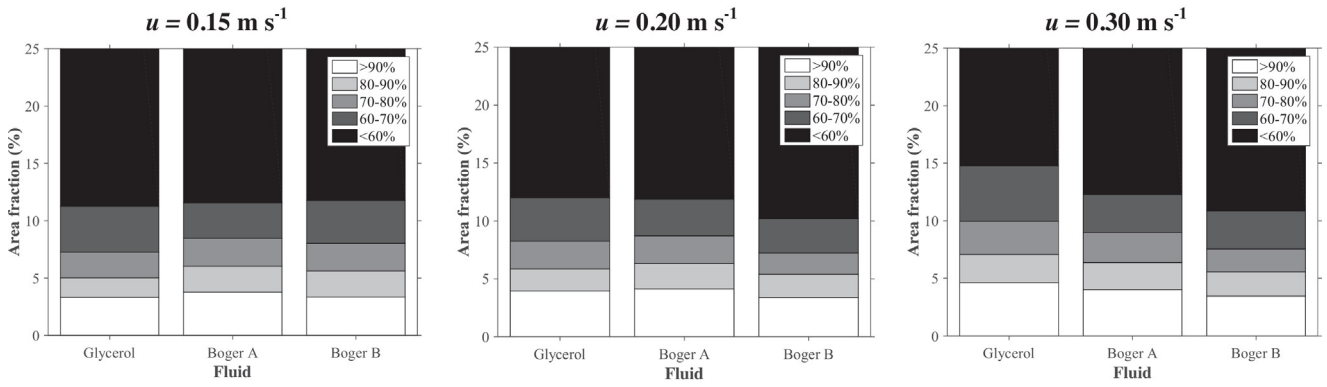

Fig. 9 – Comparison of areal mixing fractions at constant fluid velocity.

Table 3 – Time-averaged image statistics.

Velocity ($m\,s^{-1}$)	Glycerol			Boger A			Boger B		
	90% mixed fraction	Coefficient of variance CoV	Calculated mixer performance parameter, K_i	90% mixed fraction	Coefficient of variance CoV	Calculated mixer performance parameter, K_i	90% mixed fraction	Coefficient of variance CoV	Calculated mixer performance parameter, K_i
0.15	3.33 (±0.17)	0.83 (±0.01)	0.88 (±0.00)	3.77 (±0.96)	0.98 (±0.08)	0.90 (±0.00)	3.34 (±0.47)	1.13 (±0.08)	0.91 (±0.00)
0.20	3.95 (±0.30)	0.79 (±0.02)	0.88 (±0.00)	4.12 (±0.63)	1.14 (±0.11)	0.91 (±0.00)	3.38 (±0.51)	1.13 (±0.12)	0.91 (±0.00)
0.30	4.61 (±0.25)	0.78 (±0.01)	0.88 (±0.00)	4.01 (±0.71)	0.84 (±0.07)	0.88 (±0.00)	3.46 (±0.84)	1.20 (±0.13)	0.91 (±0.00)

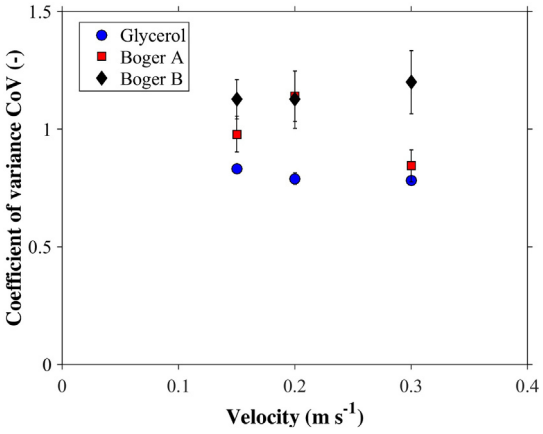

Fig. 10 – Coefficients of variance (CoV) at mixer outlet.

increase in 90% mixedness fractions as velocity increases, whilst the other fractions remain largely constant. Boger B on the other hand displays an overall decrease in the higher mixing fractions, indicating a reduction in mixing performance. This overall tendency of decreasing mixing fractions as velocity increases would appear intuitively to suggest that elasticity inhibits mixing performance. However, owing to the inverse relationship of fluid relaxation time, the key measure of elasticity in this study, and shear rate, the opposite is in fact true: as velocity increases, due to the increase in wall shear rate the fluid relaxation time decreases, indicating that the fluid would display less elastic-like behaviour at higher fluid superficial velocities. This would therefore indicate that the complex interaction of fluid elasticity and flow dynamics is causing an apparently contradictory response. It is therefore necessary to investigate the overall mixing performance against the dimensionless parameters that govern flow inertia and elasticity in order to numerically assess the impact of the flow-elasticity interaction.

3.3.2. *Assessment of trends in experimental data with dimensionless parameters*

In order to determine scaling rules and assess the governing phenomena under different process conditions, it is necessary to compare mixing data to relevant dimensionless parameters. Typically, the desired final product quality would be found using either a 90% or 95% confidence interval, and therefore in this case the 90% mixing fractions shall be taken as the required areal fraction. Further, in order to compare to other studies, the coefficient of variance shall also be assessed.

Fig. 12 displays the intensity of the 90% mixed fraction and coefficients of variance plotted against specific energy input ε.

It can be seen that there is no clear correlation between the specific energy input and the mixing performance measured through either the coefficient of variance or 90% mixed fraction. In particular, the CoV appears to show two broad trends with a reduction in this value as energy input increases for Newtonian glycerol, indicating an improvement in final mixing quality, whilst the viscoelastic Boger fluids generally show an increase in this CoV and thus a reduction in final mixing quality. This bimodal trend is seen in the areal data also, with glycerol showing an improvement in 90% mixed fraction as energy input increases, which is consistent with previous data for this mixer geometry (Alberini et al., 2013) and the traditional mixing perspective that mixing quality improves as energy input increases. However, the increase in mixing performance is much more marginal for Boger fluids, with

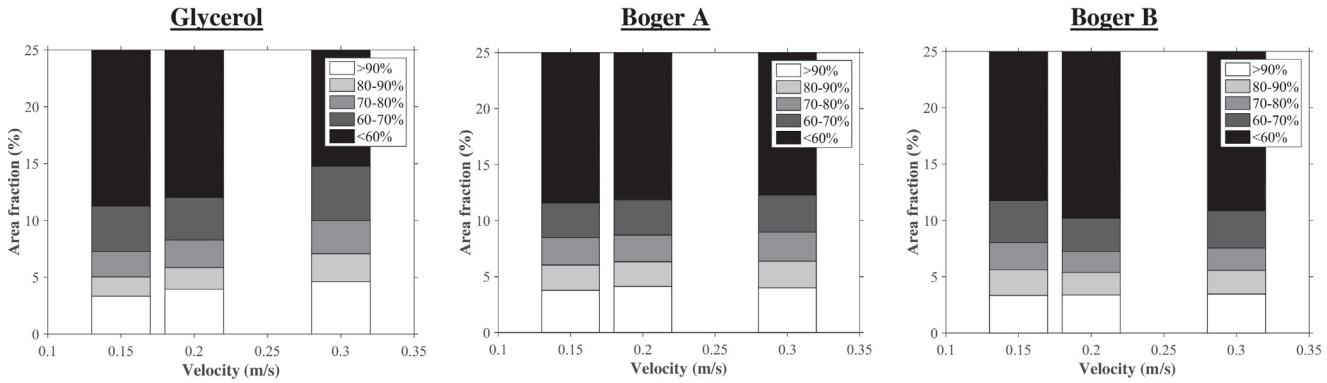

Fig. 11 – Comparison of areal mixing fractions at varying velocity.

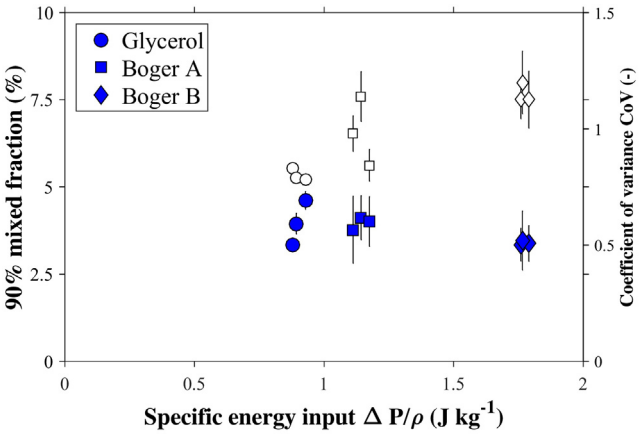

Fig. 12 – 90% mixed fraction and CoV versus specific energy input versus.

the trend suggesting no change in final mixing quality. As with the observations of pressure drop in Section 3.1, this can be attributed to the elastic storage of energy within the viscoelastic fluid, thus resulting in a lack of power dissipation contributing to mixing performance and thus no observable increase in final mixing quality across the measured range. It can therefore be concluded that using specific energy input in isolation is insufficient to predict the final mixing quality of the fluid. Thus, it is necessary to explore different parameters in order to discover an underlying controlling mixing mechanism.

Fig. 13 displays the mixing performance for all conditions against individual dimensionless numbers, assessing fluid hydrodynamics and elasticity in isolation.

As previously stated, there is no clear trend in the variation of coefficient of variance when all conditions are compared to both the Reynolds and Weissenberg numbers. Further, it can be seen that the 90% mixed fraction is fairly well correlated with Reynolds number, albeit with some outliers. The data suggest that *Re* only weakly affects the 90% mixed fraction as calculated values remain almost constant across the measured range with a slight increase at increasing values of *Re*. This is consistent with vendor guidelines, though disagrees with previous work into Newtonian fluid mixing performance, where the mixed fraction markedly increases with increasing *Re*. This discrepancy can be attributed to both the effect of fluid elasticity not being accounted for, the narrower range of Reynolds numbers investigated in this study and also the small number of mixing elements implemented. Both Boger fluids correlate well with Weissenberg number, with a slight decrease in 90% mixed fraction as *Wi* increases confirming the observation that in this mixer geometry fluid elasticity inhibits mixing performance. Owing to the inelastic nature of glycerol (i.e. $Wi = 0$) all values for this fluid are situated on the y-axis. Thus, the limitations of these parameters are apparent, as *Re* and *Wi* cannot adequately account for both elastic and inelastic fluids and therefore an approach which seeks to combine inelastic behaviour with elastic fluids should be taken.

Fig. 14 displays the same mixing performance plotted against the dimensionless groups *El* and Re_g which combine both elastic and hydrodynamic forces.

Though both plots do show strong positive correlations of mixing performance against the dimensionless parameters, Elasticity number *El* cannot predict Newtonian fluid performance as the definition of *El* includes the Weissenberg number

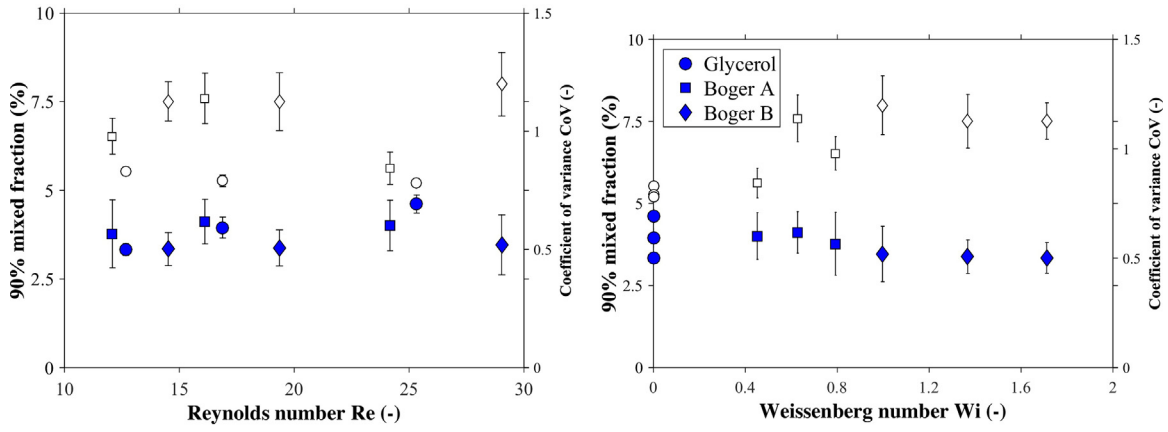

Fig. 13 – Comparison of 90% mixed fraction and coefficient of variance: (a) Reynolds number *Re*; (b) Weissenberg number *Wi*.

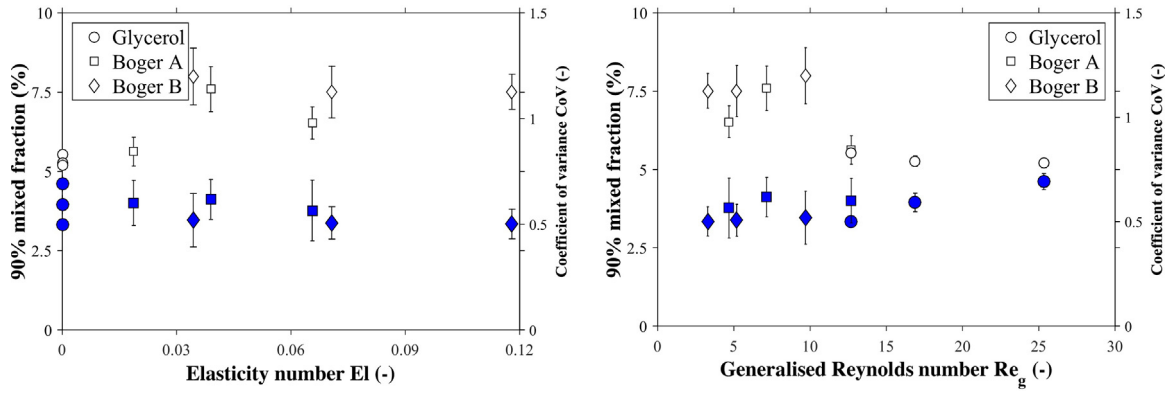

Fig. 14 – 90% mixed fraction and coefficient of variance (*CoV*): (a) elasticity number *El*; (b) generalised Reynolds number Re_g.

Wi in its definition and as previously stated this is by definition zero for inelastic fluids. The generalised Reynolds number Re_g displays a single trend upon which all fluids collapse based on the 90% mixed fraction. It clearly displays that the more elastic Boger B displays the lowest values of Re_g and mixing fraction, with inelastic glycerol possessing the greatest mixing fraction of highest values of Re_g. As velocity increases the generalised Reynolds number also increases, and additionally mixing performance in the 90% mixed fraction also increases. This is in line with the results obtained for Newtonian and non-Newtonian inelastic fluids in previous studies (Alberini et al., 2013, 2014), and suggests that increasing fluid velocity increases mixing performance whilst increasing fluid elasticity inhibits mixing. However, it must be stressed that this is a weak effect as the increase in 90% mixed fraction is only 2% of the total across the measured Re_g range.

Both *El* and Re_g show a monotonic trend in mixing performance as each parameter increases, indicating that the experimental data all falls within one particular elastic regime. As previously noted, these values fall within the unsteady flow regime as predicted by Stokes et al. (2001) for both Boger fluids, with glycerol being an "inertially" driven laminar flow governed by *Re* alone. Given the large time variation in the data it is expected that all experiments for the Boger fluids are in an unsteady flow regime, despite the lack of data to determine the transition values between elastic, inertial and unsteady flows. The trends observed may therefore not be valid in other flow regimes, though further experimentation with a wider range of fluid elasticities and Weissenberg numbers is required to confirm this.

The above dimensionless groups therefore lead to the conclusion that the primary variable that determines mixing quality is the generalised Reynolds number Re_g. Though applicable across a wider range of fluids than *Wi* or *El*, Re_g possesses several key limitations. Firstly, the concept was developed for use in stirred tank systems with second-order fluids, and as such uses a very specific definition of the Weissenberg number as a result of this. To date Re_g has not been implemented in systems with non-second-order fluids or in non-stirred tank systems, and as such there is no additional evidence beyond this study to confirm the applicability of Re_g outside of these geometries. Additionally, a relatively small range of flow conditions were implemented in this particular study owing to equipment limitations, and as such further study is required in order to validate the application of this dimensionless number to a much wider range of process conditions. Further, as strictly Re_g is merely a correction for viscoelastic power input to the process, it should only be used after other parameters have failed to fully describe the flow situation, as is the case above.

4. Conclusions

Upon investigation of the mixing performance of Newtonian and viscoelastic fluids in a Kenics KM static mixer, it has been found that viscoelasticity significantly affects the mixing performance of fluids at the outlet of a 6-element Kenics KM static mixer. This manifests as a change in striation pattern from a typical lamellar structure associated with the Kenics' helical twist element design towards a more segregated and amorphous structure. Further, the temporal variation in striation structure when a viscoelastic fluid is processed has not been previously reported, and thus elucidates a previously unknown phenomenon that has serious implications for further downstream processing. Statistical assessment of mixing performance has shown that elasticity inhibits mixing to a small degree, with the generalised Reynolds number Re_g presenting the best parameter for determining mixing performance at the outlet.

The results presented represent the first investigation into mixing performance using viscoelastic fluids. Further study should include the effect of mixer scale, i.e. the internal diameter of the pipeline containing the static mixer, and should also investigate the effect of additional mixing elements. Also, implementing higher superficial velocities within the mixer, and thus extend the study to the upper limit of the laminar flow regime, would determine the validity of these observations across the entire laminar region.

Acknowledgements

John Ramsay is funded by an EPSRC Doctoral Training Grant (EP/K502984/1) from the University of Birmingham and Johnson Matthey.

Appendix A. Derivation of generalised Reynolds number Re_g

The reasoning presented below follows the same reasoning as in Bertrand et al. (2002), where the concept of correcting the Reynolds number for viscoelastic effects was first introduced.

For a pipe system, the relationship between wall shear stress τ_w and pressure drop ΔP is given by:

$$\tau_w = \frac{\Delta P}{L}\frac{r}{2} \tag{17}$$

where r is the radius. For a second-order fluid, the stress is given as:

$$\tau = \mu\dot{\gamma} + \psi_1\dot{\gamma}^2 \tag{18}$$

Or, in a rearranged form:

$$\tau = \mu\dot{\gamma}\left(1 + \frac{\psi_1}{\mu}\dot{\gamma}\right) = \mu\dot{\gamma}(1 + 2\lambda\dot{\gamma}) = \tau_{Newtonian}(1 + 2Wi)$$
$$= \tau_{Newtonian}(1 + Wi') \tag{19}$$

Where $Wi' = 2Wi$. This can then be substituted into Eq. (17), and substituting for the friction factor:

$$\Delta P = 2\rho u^2\left(\frac{L}{D}\right) f_D(1 + Wi') \tag{20}$$

In laminar flow, $f_D = 64/Re$, obtaining:

$$\Delta P = 128\rho u^2\left(\frac{L}{D}\right)\frac{(1 + Wi')}{Re} \tag{21}$$

The expression $\frac{Re}{1+Wi'}$ is the generalised Reynolds number Re_g, which corrects the viscous term in the Reynolds number for the additional elastic stress term. Strictly speaking Re_g should only be used to correct the pressure drop in viscoelastic fluid flows, in the same way that the Metzner-Otto correlation in stirred tanks only strictly corrects the power draw for non-Newtonian fluids, and caution should be taken when used outside of this specific application. This derivation assumes that the shear rate is the same as for Newtonian fluid flow in a pipeline, which is typically corrected for in static mixers through the use of a factor K_G.

References

Barnes, H., 2003. A review of the rheology of filled viscoelastic systems. Rheol. Rev., 1–36.

Ihejirika, I., Ein-Mozaffari, F., Using, C.F.D., 2007. and ultrasonic velocimetry to study the mixing of pseudoplastic fluids with a helical ribbon impeller. Chem. Eng. Technol. 30, 606–614.

Chavan, V.V., 1983. Close-clearance helical impellers: a physical model for newtonian liquids at low Reynolds numbers. AIChE J. 29, 177–186.

Chhabra, R., Bouvier, L., Delaplace, G., Cuvelier, G., Domenek, S., Andre, C., 2007. Determination of mixing times with helical ribbon impeller for non-Newtonian viscous fluids using an advanced imaging method. Chem. Eng. Technol. 30, 1686–1691.

Jahangiri, M., 2007. Velocity distribution of helical ribbon impeller in mixing of polymeric liquids in the transition region. Iranian Polym. J. 16, 731–739.

Ramsay, J., Simmons, M.J.H., Ingram, A., Stitt, E.H., 2016. Mixing of Newtonian and viscoelastic fluids using 'butterfly' impellers. Chem. Eng. Sci. 139, 125–141.

Paul, E.L., Atiemo-Obeng, V.A., Kresta, S.M., 2003. Handbook of Industrial Mixing. John Wiley & Sons.

Rahmani, R.K., Keith, T.G., Ayasoufi, A., 2006. Numerical simulation and mixing study of pseudoplastic fluids in an industrial helical static mixer. J. Fluids Eng. Trans. ASME 128, 467–480.

van Wageningen, W.F.C., Kandhai, D., Mudde, R.F., van den Akker, H.E.A., 2004. Dynamic flow in a Kenics static mixer: an assessment of various CFD methods. AIChE J. 50, 1684–1696.

Rauline, D., Le Blevec, J.M., Bousquet, J., Tanguy, P.A., 2000. A comparative assessment of the performance of the Kenics and SMX static mixers. Chem. Eng. Res. Design 78, 389–396.

Avalosse, T., Crochet, M.J., 1997. Finite-element simulation of mixing. 2. Three-dimensional flow through a kenics mixer. AIChE J. 43, 588–597.

Regner, M., Ostergren, K., Tragardh, C., 2006. Effects of geometry and flow rate on secondary flow and the mixing process in static mixers - a numerical study. Chem. Eng. Sci. 61, 6133–6141.

Saatdjian, E., Rodrigo, A.J.S., Mota, J.P.B., 2012. On chaotic advection in a static mixer. Chem. Eng. J. 187, 289–298.

Hobbs, D.M., Muzzio, F.J., 1998. Optimization of a static mixer using dynamical systems techniques. Chem. Eng. Sci. 53, 3199–3213.

Shah, N.F., Kale, D.D., 1991. Pressure-drop for laminar-flow of non-Newtonian fluids in static mixers. Chem. Eng. Sci. 46, 2159–2161.

Chandra, K.G., Kale, D.D., 1992. Pressure-drop for laminar-flow of viscoelastic fluids in static mixers. Chem. Eng. Sci. 47, 2097–2100.

Li, H.Z., Fasol, C., Choplin, L., 1997. Pressure drop of Newtonian and non-Newtonian fluids across a Sulzer SMX static mixer. Chem. Eng. Res. Design 75, 792–796.

Kumar, G., Upadhyay, S.N., 2008. Pressure drop and mixing behaviour of non-Newtonian fluids in a static mixing unit. Can. J. Chem. Eng. 86, 684–692.

Laporte, M., Loisel, C., Della Valle, D., Riaublanc, A., Montillet, A., 2014. Flow process conditions to control the void fraction of food foams in static mixers. J. Food Eng. 128, 119–126.

Thakur, R.K., Vial, C., Nigam, K.D.P., Nauman, E.B., Djelveh, G., 2003. Static mixers in the process industries: a review. Chem. Eng. Res. Design 81, 787–826.

Alberini, F., Simmons, M.J.H., Ingram, A., Stitt, E.H., 2013. Use of an areal distribution of mixing intensity to describe blending of non-Newtonian fluids using PLIF. AIChE J. 60, 332–342.

Stokes, J.R., 1998. Swirling Flow of Viscoelastic Fluids. University of Melbourne.

Ozcan-Taskin, N.G., Nienow, A.W., 1995. Mixing viscoelastic fluids with axial-flow impellers - flow-fields and power-consumption. Food Bioprod. Process. 73, 49–56.

Bertrand, F., Carreau, P., La Fuente, E.B.-D., Tanguy, P.A., 2002. Mixing of viscoelastic fluids. In: Engineering and Food for the 21st Century. CRC Press.

Faes, M., Glasmacher, B., 2008. Measurements of micro- and macromixing in liquid mixtures of reacting components using two-colour laser induced fluorescence. Chem. Eng. Sci. 63, 4649–4655.

Hall, J.F., Barigou, M., Simmons, M.J.H., Stitt, E.H., 2005. Comparative study of different mixing strategies in small high throughput experimentation reactors. Chem. Eng. Sci. 60, 2355–2368.

Szalai, E.S., Arratia, P., Johnson, K., Muzzio, F.J., 2004. Mixing analysis in a tank stirred with Ekato Intermig((R)) impellers. Chem. Eng. Sci. 59, 3793–3805.

Zalc, J.M., Alvarez, M.M., Muzzio, F.J., Arik, B.E., 2001. Extensive validation of computed laminar flow in a stirred tank with three Rushton turbines. AIChE J. 47, 2144–2154.

Pianko-Oprych, P., Nienow, A.W., Barigou, M., 2009. Positron emission particle tracking (PEPT) compared to particle image velocimetry (PIV) for studying the flow generated by a pitched-blade turbine in single phase and multi-phase systems. Chem. Eng. Sci. 64, 4955–4968.

Gabriele, A., Nienow, A.W., Simmons, M.J.H., 2009. Use of angle resolved PIV to estimate local specific energy dissipation rates for up- and down-pumping pitched blade agitators in a stirred tank. Chem. Eng. Sci. 64, 126–143.

Stobiac, V., Fradette, L., Tanguy, P.A., Bertrand, F., 2014. Pumping characterisation of the maxblend impeller for Newtonian and strongly non-Newtonian fluids. Can. J. Chem. Eng. 92, 729–741.

Kling, K., Mewes, D., 2004. Two-colour laser induced fluorescence for the quantification of micro- and macromixing in stirred vessels. Chem. Eng. Sci. 59, 1523–1528.

Arratia, P.E., Muzzio, F.J., 2004. Planar laser-induced fluorescence method for analysis of mixing in Laminar flows. Ind. Eng. Chem. Res. 43, 6557–6568.

Alvarez, M.M., Zalc, J.M., Shinbrot, T., Arratia, P.E., Muzzio, F.J., 2002. Mechanisms of mixing and creation of structure in laminar stirred tanks. AIChE J. 48, 2135–2148.
Chung, K.H.K., Simmons, M.J.H., Barigou, M., 2009. Angle-resolved particle image velocimetry measurements of flow and turbulence fields in small-scale stirred vessels of different mixer configurations. Ind. Eng. Chem. Res. 48, 1008–1018.
Guillard, F., Tragardh, C., Fuchs, L., 2000. A study on the instability of coherent mixing structures in a continuously stirred tank. Chem. Eng. Sci. 55, 5657–5670.
Shervin, C.R., Raughley, D.A., Romaszewski, R.A., 1991. Flow visualization scaleup studies for the mixing of viscoelastic fluids. Chem. Eng. Sci. 46, 2867–2873.
Fradette, L., Thome, G., Tanguy, P., Takenaka, K., 2007. Power and mixing time study involving a Maxblend (R) impeller with viscous Newtonian and non-Newtonian fluids. Chem. Eng. Res. Design 85, 1514–1523.
Rafiee, M., Bakalisa, S., Fryer, P.J., Ingram, A., 2011. Study of laminar mixing in kenics static mixer by using Positron Emission Particle Tracking (PEPT). Procedia Food Sci. 1, 678–684.
Mihailova, O., Lim, V., McCarthy, M.J., McCarthy, K.L., Bakalis, S., 2015. Laminar mixing in a SMX static mixer evaluated by positron emission particle tracking (PEPT) and magnetic resonance imaging (MRI). Chem. Eng. Sci. 137, 1014–1023.
Kukukova, A., Aubin, J., Kresta, S.M., 2009. A new definition of mixing and segregation: three dimensions of a key process variable. Chem. Eng. Res. Design 87, 633–647.
Danckwerts, P.V., 1958. The effect of incomplete mixing on homogeneous reactions. Chem. Eng. Sci. 8, 93–102.
Stamatopoulos, K., Batchelor, H.K., Alberini, F., Ramsay, J., Simmons, M.J.H., 2015. Understanding the impact of media viscosity on dissolution of a highly water soluble drug within a USP 2 mini vessel dissolution apparatus using an optical planar induced fluorescence (PLIF) method. Int. J. Pharmaceut. 495, 362–373.
Fontaine, A., Guntzburger, Y., Bertrand, F., Fradette, L., Heuzey, M.C., 2013. Experimental investigation of the flow dynamics of rheologically complex fluids in a Maxblend impeller system using PIV. Chem. Eng. Res. Design 91, 7–17.
Seyssiecq, I., Tolofoudye, A., Desplanches, H., Gaston-Bonhomme, Y., 2003. Viscoelastic liquids in stirred vessels - Part I: Power consumption in unaerated vessels. Chem. Eng. Technol. 26, 1155–1165.
Boger, D.V., Yeow, Y.L., 1992. The impact of ideal elastic liquids in the development of non-Newtonian fluid-mechanics. Exp. Thermal Fluid Sci. 5, 633–640.
Mackay, M.E., Boger, D.V., 1987. An explanation of the rheological properties of Boger fluids. J. Non-Newtonian Fluid Mech. 22, 235–243.
James, D.F., Yip, R., Currie, I.G., 2012. Slow flow of Boger fluids through model fibrous porous media. J. Rheol. 56, 1249–1277.
Magda, J.J., Lou, J., Baek, S.G., Devries, K.L., 1991. Second normal stress difference of a Boger fluid. Polymer 32, 2000–2009.
Stokes, J.R., Graham, L.J.W., Lawson, N.J., Boger, D.V., 2001. Swirling flow of viscoelastic fluids. Part 2. Elastic effects. J. Fluid Mech. 429, 117–153.
Stokes, J.R., Boger, D.V., 2000. Mixing of viscous polymer liquids. Phys. Fluids 12, 1411–1416.
Barnes, H.A., 2000. A Handbook of Elementary Rheology. University of Wales, Institute of Non-Newtonian Fluid Mechanics.
Alberini, F., Simmons, M.J.H., Ingram, A., Stitt, E.H., 2014. Assessment of different methods of analysis to characterise the mixing of shear-thinning fluids in a Kenics KM static mixer using PLIF. Chem. Eng. Sci. 112, 152–169.
Kukukova, A., Noel, B., Kresta, S.M., Aubin, J., 2008. Impact of sampling method and scale on the measurement of mixing and the coefficient of variance. AIChE J. 54, 3068–3083.
Kukukova, A., Aubin, J., Kresta, S.M., 2011. Measuring the scale of segregation in mixing data. Can. J. Chem. Eng. 89, 1122–1138.
Grace, H.P., 1982. Dispersion phenomena in high viscosity immiscible fluid systems and application of static mixers as dispersion devices in such systems. Chem. Eng. Commun. 14, 225–277.